Journal of Medical Systems (2019) 43: 322
https://doi.org/10.1007/s10916-019-1459-2

IMAGE & SIGNAL PROCESSING

Segmentation and Diagnosis of Liver Carcinoma Based on Adaptive Scale-Kernel Fuzzy Clustering Model for CT Images

Jianhong Cai [1]

Received: 17 July 2019 / Accepted: 11 September 2019 / Published online: 10 October 2019
© Springer Science+Business Media, LLC, part of Springer Nature 2019

Abstract
Medical image analysis plays an important role in computer-aided liver-carcinoma diagnosis. Aiming at the existing image fuzzy clustering segmentation being not suitable to segment CT image with non-uniform background, a fast robust kernel space fuzzy clustering segmentation algorithm is proposed. Firstly, the sample in euclidean space is mapped into the high dimensional feature space through the kernel function. Then the linear weighted filtering image is obtained by combining the current pixel with its neighborhood pixels through the space information in CT image. Finally, the two-dimensional histogram between the clustered pixel and its neighborhood mean is introduced into the robust kernel space image fuzzy clustering, and the iterative expression of the fast robust fuzzy clustering in kernel space is obtained by using Lagrange multiplier method. The experimental results on four databases show that our proposed method can segment liver tumors from abdominal CT volumes effectively and automatically, and the comprehensive segmentation performance of the proposed method is superior to that of several existing methods.

Keywords Liver carcinoma · Scale-kernel space · Fuzzy clustering · Linear weighted filtering · Lagrange multiplier · European space · Non-uniform background

Introduction

Medical image analysis plays an important role in computer-aided diagnosis. Medical image segmentation is one of the cores of medical image analysis, whose purpose is to identify the anatomical structures of human organs from the surrounding tissues. Computed tomography (CT) images provide images of anatomical structures with high definition and high signal-to-noise ratio for clinical diagnosis in a non-invasion way [1–3]. In the area of CT-based clinical hepatic diagnosis, accurate and reliable segmentation of liver and liver tumor is essential for the follow-up treatment planning, evaluation and computer-assisted surgery. However, in existing clinical practice, manual delineation of liver and liver tumor on each slice is still typically performed by radiologists, which could obtain the arguably most accurate segmentation results, but is time-consuming, tedious, and laborious, and introduces inter-observer variability [4]. Additionally, due to the blurry edges, low level of contrast and intensity in homogeneity characterizing the CT images, accurate segmentation of liver and liver tumor is regarded as difficult work, and the segmentation method is a research highlight in the area of medical image processing.

Liver diseases are common diseases that threaten human health worldwide, which are various in variety and rapid in development. In addition, many liver diseases are not easy to heal and recover. When we do the liver segmentation, the traditional manual segmentation method depends much on the doctors' work experience and prior knowledge, which may lead to different conditions in the operation and preoperative analysis, so the success rate of the operation will not be very high [5]. If computerized image processing technology and 3D reconstruction technology can accurately segment and reconstruct the abdominal CT slice image, the sagittal and coronal images can be extracted and calculated, so that the clinician can accurately grasp the data before surgery, the success rate of surgery will be improved to some extent. Therefore, the image processing in the computer field is combined with the three-dimensional reconstruction technology and the anatomy and diagnostic technology in the medical

This article is part of the Topical Collection on *Image & Signal Processing*

✉ Jianhong Cai
caijianhongls@163.com

[1] School of Computer and Information Engineering, Hubei University, Wuhan 430064, Hubei, China

field to realize the liver CT image sequence processing and three-dimensional reconstruction, and complete the computer-aided treatment of liver diseases. It has become a hot topic at home and abroad [6].

Image segmentation is to divide the image into different regions so as to solve the pixel classification problem with similar characteristics, which is a key step in image processing and image analysis. Since the image detail will be lost when the image is projected from a three-dimensional object to a planar space, the human eye has uncertainty about the distinction between adjacent gray levels, which makes the fuzzy clustering widely used in the field of image segmentation [7]. At present, fuzzy C-means (FCM) clustering is one of the most commonly used clustering methods in image segmentation. However, the segmentation information corresponding to this cluster only uses the membership degree to express the sample classification degree, which cannot characterize the liver feature. The uncertainty and refusal degree in the sample classification make the algorithm difficult to effectively cluster complex non-convex data. To solve this deficiency, Indian scholar Chaira et al. extended the traditional fuzzy C-means clustering to the intuitionistic fuzzy set, and proposed Intuitionistic fuzzy c-means (IFCM), which not only considers the fuzzy membership degree of sample clustering, but also considers the uncertainty of its membership degree. It maximizes the classification membership degree and achieves the purpose of improving clustering performance [8]. However, increasing the membership of sample classification without principle will lead to samples misclassification with higher probability, which is not conducive to the need for complex image segmentation such as uneven gray, noise interference and so on.

In literature [6], the graphical fuzzy set is introduced into the traditional fuzzy C-means clustering algorithm, and the graphical fuzzy membership degree, neutrality and refusal degree in the clustering process is constrained, and an image fuzzy clustering algorithm is obtained, which is called as Fuzzy clustering method based on image fuzzy sets. In this clustering, only membership degree and neutrality are obtained by Yager complement operator, which results in negative values of membership degree, neutrality degree and clustering center obtained by alternating iteration, and makes the clustering algorithm invalid. Later, Thong et al. proposed an improved fuzzy clustering of image fuzzy sets, which has a certain degree of improvement compared with the existing FCM algorithm [9].

Although graphical fuzzy clustering has been successfully applied to the segmentation of medical images, its clustering only considers the grayscale information of pixels and ignores the influence of neighborhood pixel space and grayscale information on clustering, which causes the algorithm cannot suppress noise. For this reason, the literature [10] combined the neutrality and the refusal degree in the literature [7], constructs a regularization term expression. In addition, it also introduces pixel neighborhood gray information, so a robust graphical fuzzy clustering segmentation algorithm with spatial constraints is proposed. Similarly, it also can be introduced into the literature [7] to obtain an improved graphical fuzzy clustering algorithm with spatial constraints. The algorithm uses the Euclidean distance to construct the clustering objective function, which brings together similar samples in the sample space. However, it is easy to fall into the local minimum point and is sensitive to the initialization value. It is mainly suitable for the class that the clustering data sets with different sample numbers are not disparate, and the clustering performance is significantly reduced for clustering of non-convex data. The kernel-based fuzzy c-means clustering method (KFCM) clustering algorithm can effectively solve the non-convex data clustering problem, which maps the sample data to the high-dimensional feature space and improves the reparability of the sample to achieve the purpose of improving clustering performance [11]. However, the introduction of the kernel function will increase the computation complexity of the algorithm, which is not conducive to the need for image segmentation in the case of high real-time requirements for medicine image. Therefore, literature [12] proposed a fast FCM segmentation algorithm for spatial information constraints, which uses the grayscale and spatial position information in the neighborhood window of each pixel of the original image to construct a new linear weighted image. Then, image clustering is performed on the gray histogram of the image to reduce the running time, and the noise suppression capability is improved, but the segmentation performance of the segmentation algorithm cannot be improved, which is disadvantageous for image segmentation in complex occasions such as medicine image [13–15].

In order to improve the segmentation performance and noise suppression ability of the robust graphics fuzzy clustering segmentation method and reduce the time overhead of large-scale medical image segmentation, this paper extends the fuzzy clustering method on image fuzzy sets with spatial constraints (FCSC) to the kernel space and combines it with the fast generalized FCM (FGF) segmentation algorithm. An improved robust kernel space graph fuzzy clustering segmentation algorithm is proposed, and a two-dimensional histogram closely related to pixels and its neighboring pixels is introduced into the new robust segmentation algorithm to obtain a fast robust kernel space image fuzzy clustering segmentation algorithm. The test results show that the proposed algorithm can effectively improve the segmentation speed of medicine images. In addition, it can have a stronger segmentation performance than the existing fuzzy clustering segmentation method. The application of the algorithm proposed in this paper to ten sets of abdomen CT images with blur edge for liver segmentation proved the adaptability and effectiveness of our approach for complex image segmentation.

Materials and methods

Related works

In order to reduce the complexity of liver tumor extraction and improve the accuracy of liver tumor extraction, literature [16] preprocesses abdominal CT sequence images. First, the initial contour of liver is obtained by using three-dimensional filtering and convex-hull algorithm. Then, the sparse shape combination based on multi-level local region is used to optimize the contour of liver and obtain the liver region in CT image, namely liver masking. This paper mainly focuses on the automatic segmentation of tumors in the liver region of abdominal CT sequence images. Figure 1 shows the flow-chart of the liver segmentation and tumor diagnosis. First, the liver masking in abdominal CT images is obtained by preprocessing, and then the gray probability distribution of the liver region is obtained according to the liver masking. Segmental non-linear enhancement is used to improve the contrast between tumors and normal liver parenchyma, and then the image segmentation energy function based on multi-objective segmentation is constructed by using the enhancement results combined with image gradient information [17]. Finally, the segmentation results are optimized by three-dimensional morphological opening operation to remove the wrong segmentation areas and obtain the results. The final segmentation results of liver tumors are obtained.

According to the characteristics of CT scanning and the fact that the tissues and organs in abdominal CT images are usually located in a narrow gray-scale range, and the gray-scale distribution is Gauss distribution [18]. In order to obtain the gray-scale distribution range of the liver region, the liver region in abdominal CT sequence images is first obtained by using liver masking, and then Gauss function is used to fit the gray probability distribution of the whole liver region. However, the shapes and contours of liver images at different locations are quite different, and can not be directly simulated by Gauss distribution [19, 20].

The approximate location of each cross-sectional slice is indicated in Fig. 2. From top to bottom cross-section slices, the area of the liver must be from minimum to maximum to minimum, and the results are shown in Fig. 3 as follows:

For segmentation of the liver portion of a CT image sequence, it is very efficient and necessary to use different sequences with different algorithms. In some literature [21–25], the liver is usually the largest region, and the slices with smaller liver area are ignored. For example, the literature [24] uses the histogram threshold value method and the maximum connection component algorithm to segment the liver, so when the liver area is small. There will be cases where the other areas are mistakenly segmented.

Fuzzy clustering

Fuzzy clustering is the process of dividing a set of data sets into categories by a specified feature without training samples. In digital image segmentation, features are generally image gray-scale, color, texture, and so an. Fuzzy C-value clustering (fuzzy C-means, FCM) is the most commonly used fuzzy clustering method and is widely used in image segmentation [26].

The FCM algorithm is derived from k-means clustering. The k-means clustering classifies the data set X into a k-class according to the data element x attribute. In image segmentation, N is equal to the number of pixels. K-means clustering can be achieved by minimizing the cost function as follows:

$$J = \sum_{i=1}^{k}\sum_{j=1}^{N}\left\|x_j - v_i\right\|_2^2 \quad (1)$$

where x_j is the image pixel value, v_i is the center of the ith class. When the variance between classes is the largest and the variance within the class is the smallest, the cost function takes the minimum value.

The k-means clustering is a kind of hard segmentation, and one data element belongs to only one class. In contrast, FCM clustering is a kind of soft segmentation, which uses the membership function u_{ij} to characterize the extent to which the data element x_j belongs to the ith class. The cost function of FCM is as follows:

$$J = \sum_{i=1}^{C}\sum_{j=1}^{N}u_{ij}^{l}\left\|x_j - v_i\right\|_2^2 \quad (2)$$

where C is the number of categories, l is the fuzzy control parameter ($l > 1$).

Proposed liver segmentation and its cancer region detection model

In order to improve the segmentation performance and noise suppression ability of robust image fuzzy clustering

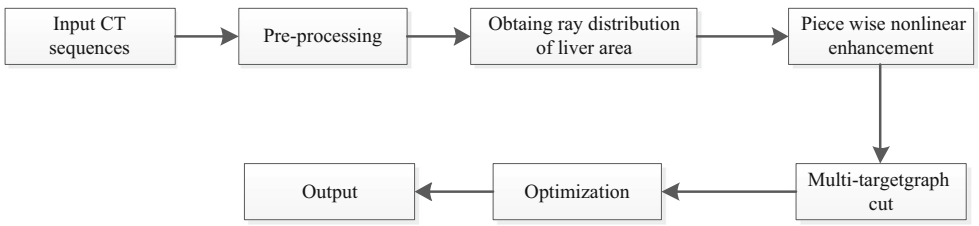

Fig. 1 Traditional flow-chart for the liver segmentation and tumor diagnosis

segmentation method and reduce the time complexity of medical image segmentation, this paper extends the fuzzy clustering method on image fuzzy sets to kernel space and combines it with segmentation method, and proposes an improved robust kernel space image fuzzy clustering segmentation method. And a fast and robust kernel space image fuzzy clustering segmentation method is obtained by introducing a two-dimensional histogram whose pixels have close relation with its neighboring pixels into the new robust segmentation method. The test results show that the proposed method can effectively improve the speed of large-scale image segmentation, and has stronger segmentation performance than the existing image fuzzy clustering segmentation method.

Robust image fuzzy clustering

In view of the problem of negative value existed in refusal degree of FCMFC method, the membership degree, neutrality and clustering center appear illegal values, and lack of robust anti-noise. Literature [20] constructs an FCMFC with spatial constraints method based on the regularization idea of neutrality and refusal degree in Literature [27] and introducing the mean value information of pixel in the neighborhood region. The optimal model of FCMFC with spatial constraints is as follows:

$$\min J(U,V,\eta,\xi)=\sum_{i=1}^{n}\sum_{k=1}^{c}\left(\frac{u_{i,k}}{1-\eta_{i,k}-\xi_{i,k}}\right)^{m}\left[(x_i-v_k)^2+a\left(\bar{x}_i-v_k\right)^2\right] \quad (3)$$
$$+\sum_{i=1}^{n}\sum_{k=1}^{c}\left(\xi_i,\eta_{i,k}^2+\xi_{i,k}^2\eta_{i,k}\right)$$

The constraints conditions of the objective function are as follows:

1) $0\le u_{i,k},\eta_{i,k},\xi_{i,k}\le 1, 0\le u_{i,k}+\eta_{i,k}+\xi_{i,k}\le 1, i=1,2,\ldots, n, k=1,2,\ldots,c;$
2) $\sum_{k=1}^{c}\frac{u_{i,k}}{1-\eta_{i,k}-\xi_{i,k}}=1, i=1,2,\ldots n;$
3) $\sum_{k=1}^{c}\left(\eta_{i,k}+\frac{1}{c}\xi_{i,k}\right)=1, i=1,2,\ldots\ldots$

where n denotes the number of clustering samples; c denotes the number of clustering clusters; $u_{i,k}$, $\eta_{i,k}$, $\xi_{i,k}$ denotes the membership degree, neutrality degree and refusal degree of class k in the i-th sample x_i, respectively; x_i denotes the i-th sample, where $\bar{x}_i$ denotes the mean value of the sample in the neighboring window corresponding to the current sample x_i; v_k denotes the clustering center of class k; $(x_i-v_k)^2$ denotes the Euclidean distance between the sample x_i and the clustering center v_k; $(\bar{x}_i-v_k)^2$ denotes the square of Euclidean distance between the mean value $\bar{x}_i$ and the clustering center v_k; m is a fuzzy index, and usually $m=2$; α is a parameter describing the influence of pixel information in neighboring area on the current pixel clustering segmentation.

Kernel-based robust image fuzzy clustering

For the optimization model in Eq. (3), its corresponding iterative clustering method is mainly suitable for clustering data analysis. In order to enhance the adaptability of the clustering model to the clustering data of different shapes, the data samples are mapped to the high-dimensional Hilbert kernel space [28] through the non-linear function $\Phi(\cdot)$. It has an inner product relationship $K(x,y)=\langle\Phi(x),\Phi(y)\rangle$ with the kernel function. By changing the spatial distribution structure between samples, the performance of fuzzy clustering is improved. The corresponding optimization model of kernel-based FCMFC with spatial constraints (FCSC) is as follows:

$$\min J(U,V,\eta,\xi)=\sum_{i=1}^{n}\sum_{k=1}^{c}\left(\frac{u_{i,k}}{1-\eta_{i,k}-\xi_{i,k}}\right)^{m}\left[d_\Phi^2(x_i,v_k)+ad_\Phi^2\left(\bar{x}_i,v_k\right)^2\right] \quad (4)$$
$$+\sum_{i=1}^{n}\sum_{k=1}^{c}\left(\xi_i,\eta_{i,k}^2+\xi_{i,k}^2\eta_{i,k}\right)$$

The constraints of the model are the same as those of the optimization model in Eq. (3). Where $d_\Phi^2(x_i,v_k)=\|\Phi(x_i)-\Phi(v_k)\|^2$ denotes the square Euclidean distance between $\Phi(x_i)$ and $\Phi(v_k)$; $d_\Phi^2(\bar{x}_i,v_k)=\|\Phi(\bar{x}_i)-\Phi(v_k)\|^2$ denotes the square Euclidean distance between $\Phi(\bar{x}_i)$ and $\Phi(v_k)$; $\Phi(x_i)$ and $\Phi(v_k)$ denote the image of sample x_i and clustering center v_k in high-dimensional feature space, respectively. Kernel function K (x, y) often chooses the Gauss kernel function $K_\sigma(x,y)=\exp(-\sigma^{-2}\cdot\|x-y\|^2)$ (σ is the parameter of the kernel function), so there is $d_\Phi^2(x_i,v_k)=2(1-K_\sigma(x_i,v_k))$. The iteration expressions of membership degree, neutrality degree, and clustering center corresponding to optimal Eq. (4) are as follows:

$$u_{i,k}=\frac{1-\eta_{i,k}-\xi_{i,k}}{\sum_{j=1}^{c}\left(\frac{d_\Phi^2(x_i,v_k)+\alpha d_\Phi^2\left(\bar{x}_i,v_k\right)}{d_\Phi^2\left(x_i,v_j\right)+\alpha d_\Phi^2\left(\bar{x}_i,v_j\right)}\right)^{\frac{1}{m-1}}} \quad (5)$$

$$\eta_{i,k}=\xi_{i,k}\left(2\eta_{i,k}+\xi_{i,k}\right)/\left(c\left(\eta_{i,k}+2\xi_{i,k}\right)\right) \quad (6)$$

$$\xi_{i,k}=1-\left(u_{i,k}+\eta_{i,k}\right)-\left(1-\left(u_{i,k}+\eta_{i,k}\right)^{\beta}\right)^{1/\beta} \quad (7)$$

$$v_k=\frac{\sum_{i=1}^{n}\left(\frac{u_{i,k}}{1-\eta_{i,k}-\xi_{i,k}}\right)^{m}\left(K_{\sigma_1}(x_i,v_k)x_i+\alpha K_{\sigma_2}\left(\bar{x}_i,v_k\right)\bar{x}_i\right)}{\sum_{i=1}^{n}\left(\frac{u_{i,k}}{1-\eta_{i,k}-\xi_{i,k}}\right)^{m}\left(K_{\sigma_1}(x_i,v_k)+\alpha K_{\sigma_1}\left(\bar{x}_i,v_k\right)\right)} \quad (8)$$

where $\beta\in(0,1)$ is a regulation parameter; σ_1 and σ_2 are different parameters of Gauss kernel function.

The above Eq. (4) can be extended to the FGF method, and a fast generalized kernel-based FCMFC is obtained, which makes the clustering performance much better than that of the FGFCM method.

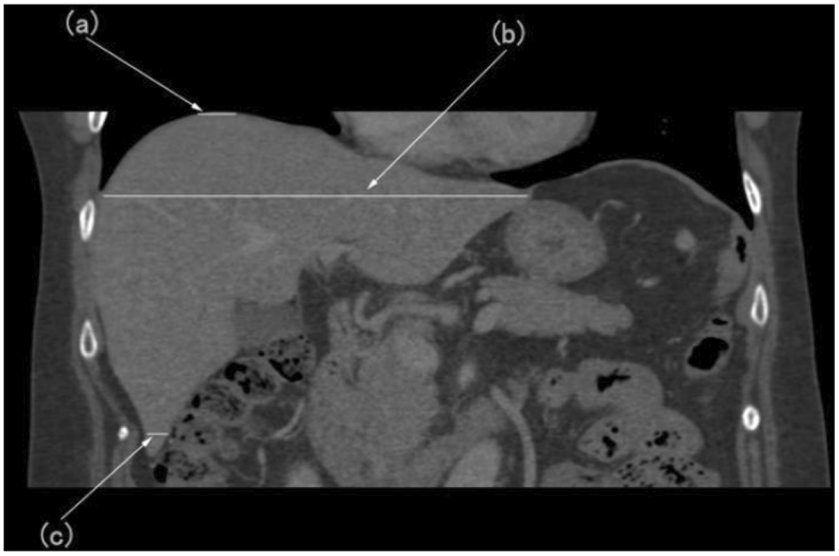

Fig. 2 Abdomen CT image. **a**, **b** and **c** are different location in image

The improved kernel-based robust image fuzzy method

In order to further improve the ability of image fuzzy clustering to suppress noise, the smoothing filtering information of neighboring pixels in literature [29] is extended to image fuzzy clustering. The corresponding optimization model is:

$$\min J(U,V,\eta,\xi)=\sum_{i=1}^{n}\sum_{k=1}^{c}\left(\frac{u_{i,k}}{1-\eta_{i,k}-\xi_{i,k}}\right)^{m}d^2(g_i,v_k)+\sum_{i=1}^{n}\sum_{k=1}^{c}\left(\xi_i,\eta_{i,k}^2+\xi_{i,k}^2\eta_{i,k}\right) \quad (9)$$

where g_i denotes the weighted image obtained by estimating all samples in the neighboring window corresponding to the current sample x_i.

Although the optimization Eq. (9) has a certain ability to suppress noise, it is difficult to meet the needs of image segmentation in complex situations such as medicine. To this end, a kernel-based robust image fuzzy clustering optimization model with stronger noise suppression ability is constructed by combining the optimization model Eqs. (4) and (9):

$$\min J(U,V,\eta,\xi)=\sum_{i=1}^{n}\sum_{k=1}^{c}\left(\frac{u_{i,k}}{1-\eta_{i,k}-\xi_{i,k}}\right)^{m}\left[d_{\Phi}^2(g_i,v_k)+\alpha d_{\Phi}^2\left(\overline{g}_i,v_k\right)\right]+\sum_{i=1}^{n}\sum_{k=1}^{c}\left(\xi_i,\eta_{i,k}^2+\xi_{i,k}^2\eta_{i,k}\right) \quad (10)$$

where $\overline{g}_i$ is obtained by estimating means of all $g_r(r\in N_i)$ in the neighborhood window corresponding to the current sample x_i.

For the optimal model in Eq. (10), the Gauss kernel function with local approximation ability is selected to obtain the iterative expressions similar with Eqs. (5) to (8). Although the corresponding segmentation method can improve the noise suppression ability of the optimal model (4), the common time-consuming shortcomings of the two methods are not conducive to the rapid segmentation of medical images.

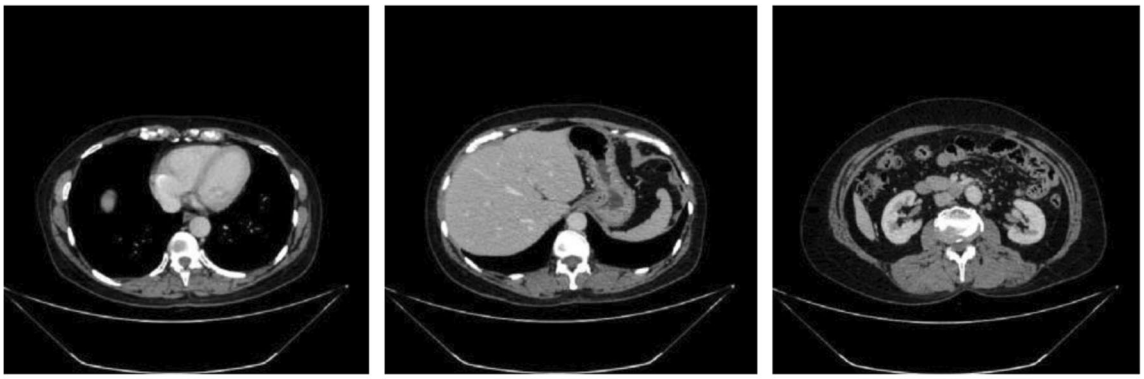

Fig. 3 Abdominal CT slices of different layer; **a** The slice with the smallest liver area form (a) in Fig. 2; **b** The slice of the largest liver in the middle layer; **c** The slice of the smallest liver in the lowest layer

Fast kernel-based image fuzzy clustering

In order to improve the speed of weighted image segmentation based on pixel neighboring information, histogram fuzzy clustering is introduced into linear weighted kernel-based robust image fuzzy clustering. And a kernel-based robust image fuzzy clustering segmentation method based on two-dimensional histogram is explored [30].

Assuming that the size of the gray image is $M_1 \times N_1$ and different gray levels are L, the image obtained by smoothing 3×3 or 5×5 neighboring template is $G^{'} = \left(g^{'}_{xy}\right)_{M_1 \times N_1}$. The two-dimensional histogram corresponding to different pixels in the same position of image G and smoothed filter image $G^{'}$ is described as follows:

$$H(i,j) = \sum_{x=1}^{M_1} \sum_{Y=1}^{N_1} \delta\left(g_{xy} - i\right) \delta\left(g^{'}_{xy} - j\right) \tag{11}$$

It describes the distribution of different gray levels in the same position of image G and its smoothed filtering image$G^{'}$, and has been widely used to solve the problem of robust segmentation of image disturbed by noise. At the same time, it can realize fast segmentation of large-scale image and has great practical value for target tracking and recognition in high real-time situations. The two-dimensional histogram obtained by combining liver image with smoothed filter image is shown in Fig. 4b.

As can be seen from Fig. 4, the two-dimensional histogram describes the spatial distribution of filtering information between any pixel of an image and its neighboring pixels. It can be used to enhance the ability of threshold segmentation or clustering segmentation to suppress noise interference. Therefore, this paper applies it to robust image fuzzy clustering segmentation algorithm and improves its real-time performance, and promotes the wide application of this algorithm in medical field [31].

Aiming at the optimal kernel-based robust image fuzzy clustering method in Eq. (8), a two-dimensional histogram is introduced and an equivalent model is obtained:

$$\begin{aligned} \min J(U,V,\eta,\xi) &= \sum_{i=1}^{M_1} \sum_{j=1}^{N_1} \sum_{k=1}^{c} \left(\frac{u_{g_{ij},k}}{1-\eta_{g_{ij},k}-\xi_{g_{ij},k}} \right)^m \times \left[d_\Phi^2\left(g_{ij}, v_k\right) + d_\Phi^2\left(\overline{g}_{ij}, v_k\right) \right] + \sum_{i=1}^{M_1} \sum_{j=1}^{N_1} \sum_{k=1}^{c} \left(\xi_{g_{ij},k} \eta^2{}_{g_{ij},k} + \xi^2{}_{g_{ij},k} \eta_{g_{ij},k} \right) \\ &= \sum_{i=0}^{L-1} \sum_{j=0}^{L-1} \sum_{k=1}^{c} H(i,j) \left(\frac{u_{i,k}}{1-\eta_{i,k}-\xi_{i,k}} \right)^m \times \left[d_\Phi^2(i,v_k) + \alpha d_\Phi^2(j,v_k) \right] + \sum_{i=0}^{L-1} \sum_{j=0}^{L-1} \sum_{k=1}^{c} H(i,j) \left(\xi_{i,k} \eta^2{}_{i,k} + \xi^2{}_{i,k} \eta_{i,k} \right) \end{aligned} \tag{12}$$

1) $0 \le u_{i,k}, \eta_{i,k}, \xi_{i,k} \le 1, 0 \le u_{i,k} + \eta_{i,k} + \xi_{i,k} \le 1, 0 \le i \le L-1, 1 \le k \le c$;
2) $\sum_{k=1}^{c} \frac{u_{i,k}}{1-\eta_{i,k}-\xi_{i,k}} = 1, \sum_{k=1}^{c} \left(\eta_{i,k} + \frac{1}{c}\xi_{i,k}\right) = 1, 0 \le i \le L-1$;
3) $0 < \sum_{i=0}^{L-1} u_{i,k}, \sum_{i=0}^{L-1} \eta_{i,k}, \sum_{i=0}^{L-1} \xi_{i,k} < L, 1 \le k \le c$.

where $g = \left(g_{xy}\right)_{M_1 \times N_1}$ is weighted by image $G = \left(g_{xy}\right)_{M_1 \times N_1}$ using the pixel neighboring information according to Eq. (10); $\overline{g} = \left(\overline{g}_{xy}\right)_{M_1 \times N_1}$ is the neighboring pixel mean filter image corresponding to image $g = \left(g_{xy}\right)_{M_1 \times N_1}$; two-dimensional histogram $H(i,j) = \sum_{x=1}^{M_1} \sum_{y=1}^{N_1} \delta\left(g_{xy} - i\right) \delta\left(\overline{g}_{xy} - j\right)$.

For the optimization model in Eq. (12), the iterative expressions of membership, neutrality and clustering center corresponding to the Gauss kernel function are as follows:

$$u_{i,k} = \frac{1-\eta_{i,k}-\xi_{i,k}}{\sum_{j=1}^{c} \left(\frac{\left(1-K_{\sigma_1}(i,v_k)\right)+\alpha\left(1-K_{\sigma_1}(j,v_k)\right)}{\left(1-K_{\sigma_1}(i,v_q)\right)+\alpha\left(1-K_{\sigma_2}(j,v_q)\right)} \right)^{\frac{1}{m-1}}} \tag{13}$$

$$\eta_{i,k} = \xi_{i,k}\left(2\eta_{i,k} + \xi_{i,k}\right) / \left(c\left(\eta_{i,k} + 2\xi_{i,k}\right)\right) \tag{14}$$

$$\xi_{i,k} = 1 - \left(u_{i,k} + \eta_{i,k}\right) - \left(1 - \left(u_{i,k} + \eta_{i,k}\right)^{\beta}\right)^{1/\beta} \tag{15}$$

$$v_k = \frac{\sum_{i=1}^{L-1} \sum_{r=1}^{L-1} H(i,r) \left(\frac{u_{i,k}}{1-\eta_{i,k}-\xi_{i,k}} \right)^m \left(K_{\sigma_1}(i,v_k) i + \alpha K_{\sigma_2}(r,v_k) r\right)}{\sum_{i=1}^{L-1} \sum_{r=0}^{L-1} H(i,r) \left(\frac{u_{i,k}}{1-\eta_{i,k}-\xi_{i,k}} \right)^m \left(K_{\sigma_1}(i,v_k) i + \alpha K_{\sigma_2}(r,v_k)\right)} \tag{16}$$

where σ_1 and σ_2 are estimated by using pixel mean square deviation of weighted sum image $G = \left(g_{xy}\right)_{M_1 \times N_1}$ and neighborhood mean smoothed image $\overline{G} = \left(\overline{g}_{xy}\right)_{M_1 \times N_1}$.

Using the above iteration expressions, a fast kernel-based robust image clustering segmentation algorithm can be constructed. The detailed processes are described as follows:

Step 1: Introducing the idea of literature [13], the weighted image $g = \left(g_{xy}\right)_{M_1 \times N_1}$ corresponding to the original segmented image $G = \left(g_{xy}\right)_{M_1 \times N_1}$ is obtained, and the local mean filter image is obtained from the weighted image $\overline{g} = \left(\overline{g}_{xy}\right)_{M_1 \times N_1}$.

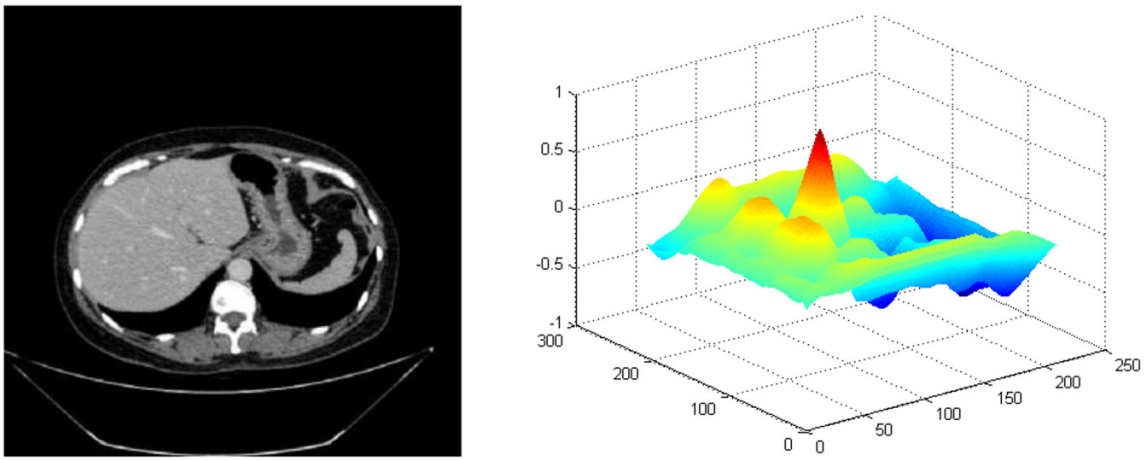

(a) (b)

Fig. 4 Liver image and its two-dimensional histogram

Step 2: using weighted image $g = \left(g_{xy}\right)_{M_1 \times N_1}$ and local mean filter image $\overline{g} = \left(\overline{g}_{xy}\right)_{M_1 \times N_1}$ to obtain two-dimensional histogram $H(i,j)(i,j = 0, 1, \ldots, L-1)$ of pixel pairs in different positions.

Step 3: using two-dimensional histogram $H(i,j)$ to calculate the parameter σ_1 of Gauss function of the weighted image and the parameter σ_2 of Gauss function of the local mean filter image.

Step 4: initialize clustering center $v_k^{(0)}$; select the number of clustering c, fuzzy index m and error of iteration final ratio ε; set initial iteration number t = 0, maximum iteration number $t_{\max} = 1000$, and choose appropriate values for parameter α and β in experience, where $\beta \in (0, 1)$.

Step 5: using the fuzzy membership degree $u_{i,\,k}$, neutrality degree $\eta_{i,\,k}$, refusal degree $\xi_{i,\,k}$ and iteration expressions of Eqs. (13), (14) and (15) to calculate the fuzzy membership degree, neutrality degree and refusal degree of corresponding gray level clustering.

Step 6: using iteration expression of clustering center v_k in Eq. (16) to renew the corresponding clustering center.

Step 7: if $\max\limits_{1 \le k \le c} \left\{ \left| v_k^{(t+1)} - v_k^{(t)} \right| \right\} > \varepsilon$ and $t + 1 < T$, add iterative time to $t = t + 1$ and turn to Step 5; or stop the clustering segmentation algorithm.

Experiment results

Data set

In order to evaluate the accuracy and performance of the proposed liver segmentation method, 60 sets of clinical portal phase abdominal enhanced CT images were used to test it. These data were collected from three open datasets and self-built dataset [32–34]. The first open data set SLIVER07 is 30 sets of CT images provided by the organizers of the 2007 International Conference on Medical Imaging Computing and Computer Aided Intervention (MICCAI Liver Segmentation Competition) [33]. It includes 20 sets of training data with Gold Standard (SLIVER07-Train) and 10 sets of test data without gold standard (SLIVER07-Test). Most of the CT images in the dataset contain liver lesions, including tumors, metastases and hepatic cysts of different sizes. The second open data set, Dircadb database, is 20 sets of CT images containing gold standard provided by the French Center for Gastrointestinal Cancer Research (IRCAD) [35]. The 15 groups of CT images in the dataset included liver lesions, including metastases, primary hepatocellular carcinoma (HCC) and hepatic hemangioma. The Dircadb database provides abdominal CT images of 10 male and 10 female patients with venous enhanced phase from different hospitals in Europe, where the liver regions of 15 sequences showed different degrees of tumor lesions. The number of planar pixels in the CT sequence slice is 512 × 512, the plane pixel pitch ranges from 0.56 to 87 mm, and the layer spacing is 1.0~4.0 mm. The HSCU database contains 10 abdominal CT with liver tumors. The sequence images were obtained from the Philips brilliance 64-row multi-slice spiral CT machine, provided by West China Hospital of Sichuan University [36]. The data was collected during the plain or vascular enhancement period. The number of pixels in the slice plane was 512 × 512, and the pixel pitch range was 0.67~0.88 mm, layer spacing is 5.0 mm. Four groups of CT images included liver lesions, including primary hepatocellular carcinoma, hepatic cyst and hepatic hemangioma, and the CT images in the data set have high image resolution.

Evaluation indexes

In this paper, Dice similarity coefficient (DSC), volume overlap error (VOE), relative volume difference (RVD), average symmetric surface distance (ASD), root square symmetric surface distance (RMSG) and maximum symmetric surface distance (MSD) are used to evaluate the results of tumor segmentation. They are defined as follows:

$$\mathrm{DSR} = \frac{2|A \cap B|}{|A| + |B|} \times 100\% \tag{17}$$

where A and B represent the liver tumor region and the real tumor region, separately; $|\cdot|$ represents the number of pixels in the given region. The larger the value of DSC, the better the segmentation performance of the algorithm.. When the segmentation result of the algorithm is identical with the real liver tumor region, the DSC value is 1. The DSC coefficient is one of the most important evaluation indexes for the performance of the algorithm.

$$\mathrm{VOE} = \left(1 - \frac{|A \cap B|}{|A \cup B|}\right) \times 100\% \tag{18}$$

The range of VOE is [0,1]. Unlike DSC, the smaller the VOE is, the better the segmentation effect is.

$$\mathrm{RVD} = \frac{|\mathrm{A}| - |\mathrm{B}|}{|B|} \times 100\% \tag{19}$$

RVD judges whether the algorithm tends to over-segmentation or under-segmentation by taking the positive and negative values. Taking the value of 0 only means that the number of pixels of A and B is equal, and does not mean that they overlap completely. Therefore, the segmentation performance of the algorithm can not be determined only by using this index.

$$\mathrm{ASD} = \frac{1}{|S(A)| + S(B)} \left(\sum_{p_a \in S(A)} d\left(\rho_a, S(B)\right) + \sum_{p_a \in S(A)} d\left(\rho_a, S(B)\right) \right) \tag{20}$$

$S\ (A)$ and $S\ (B)$ represent the surface pixel sets of A and B, respectively; and $d\ (p,\ S)$ represents the Euclidean distance between the pixel points P and the set S.

$$RMSD = \sqrt{\frac{1}{|S(A)| + S(B)}} \times \sqrt{\sum_{\rho_a \in S(A)} d^2(\rho_a, S(B)) + \sum_{\rho_a \in S(B)} d^2(\rho_a, S(\mathrm{A}))} \tag{21}$$

RMSD is highly correlated with ASD, but it is more sensitive to larger surface errors from the real liver region.

$$\mathrm{MSD} = \max\left\{ \max_{\rho_a \in S(A)} d^2(\rho_a, S(B)),\ \max_{\rho_a \in S(B)} d^2(\rho_a, S(A)) \right\} \tag{22}$$

MSD is the largest value of surface segmentation error in the sequence. The three units of surface error ASD, RMSD and MSD are all *mm*, and the smaller the value, the closer the segmentation result is to the object area.

Qualitative and quantitative analysis

In order to compare the differences of segmentation performance, noise suppression ability, time overhead for FC-PFS [12], PFCM [16], FCPFS-S1 [27], PFC [37], PKFC [28], FGPKFCM [38] algorithm and our proposed in this paper, we carried out a lot of qualitative and quantitative experimental analysis.

Due to space limitations, this paper only selected four results for analysis. In addition, two of our best algorithms are selected for qualitative comparison. Figure 5 shows the experimental results of a partial 2D slice of the 3Dircadb database. The slice contains different numbers and sizes of liver tumors. The area indicated by the white closed color curve is the segmentation result of this method, and the area marked by the black closed curve is the 3Dircadb database. The manual segmentation results are provided. It can be seen that in most cases, the method is close to the manual segmentation results, indicating that the method can achieve satisfactory segmentation results for different small, large and gray liver tumors [28]; In the case of tumor regions that are too small and have low contrast, this method is difficult to detect. In addition, in

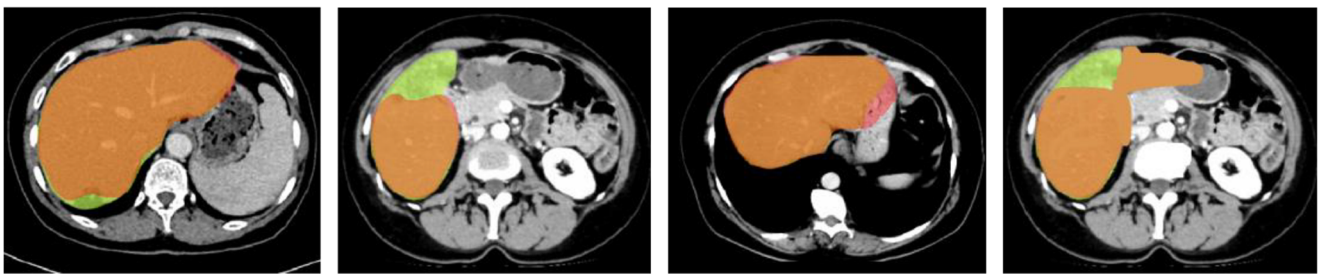

Fig. 5 The qualitative comparison among our proposed algorithm, FCM and the benchmark results, where red is the benchmark result, orange is our result, green is the FCM result

Table 1 Quantitative comparative results of the liver segmentation on the SLIVER07-Test database

Models	Dice/%	VOE	RVD/%	ASD/mm	MSD/mm	RMSD/mm	Time/s
FC-PFS	0.8439	0.2852	0.1217	3.928	31.198	12.289	121.8
PFCM	0.8687	0.2851	0.1852	2.416	28.705	17.6581	22.8
FCPFS	0.7928	0.3103	0.1624	5.497	25.510	16.9754	13.1
PFC	0.8126	0.3489	0.1552	6.259	29.325	17.028	8.2
PKFC	0.8329	0.3011	0.1524	8.555	27.125	19.253	4.8
PKFCM	0.8691	0.2875	0.1985	3.254	26.098	12.295	10.0
Proposed	0.8702	0.2793	0.1801	2.925	25.5831	11.296	3.35

the manual segmentation process, experts mark multiple tumors at close range as one tumor region, and the method uses the image grayscale and gradient information to the liver. The tumor is automatically segmented, and compared with the manual segmentation results, there is a certain degree of under-segmentation for multiple tumor regions at close range.

As can be seen from Fig. 5, if the FCM algorithm is applied to CT images with large liver area, it can achieve good segmentation effect, and can also extract the liver region almost completely. But there are also a series of changes in the liver in the CT sequence. If the liver area of the sequence in the slice is relatively small, it will lead to poor segmentation results. In addition, in the application of traditional FCM algorithm, it is easy to include kidney errors in images. The main reason is that the gray values of liver and kidney are close. In addition, this method needs to be combined with image gray value in application, and set the number of clusters and the initial clustering center in advance. It takes a lot of time in application and is also vulnerable to subjective factors.

Table 1 is a quantitative indicator of different comparison algorithms. From the test results in Table 1, the DSR value of the proposed algorithm is the smallest, indicating that the clustering performance of the proposed algorithm is superior. In addition, from the segmentation results in Fig. 5, the segmentation results obtained by the FC-PFS and PFCM algorithms have significant noise particles, while the other five algorithms have significantly enhanced anti-Gaussian noise performance compared to FC-PFS and PFCM, in which neighboring pixel grays are embedded. The graphical fuzzy clustering algorithm FCPFS, PFC, PKFCM and the proposed algorithm have a stronger robust segmentation ability than FC-PFS, which does not combine neighborhood pixel gray information. At the same time, compared with The other six algorithms, the algorithm proposed in the paper results in a clearer edge and a significant reduction in particle noise points.

In order to objectively and quantitatively evaluate the segmentation performance of each algorithm, Table 2 shows the Dice similarity coefficient and segmentation misclassification rate of Gaussian noise suppression by different algorithms. It can be seen from the peak signal-to-noise ratio and the misclassification rate in Table 2 that the algorithm with neighborhood information has higher Dice similarity coefficient (DSC), and lower volume overlap error, but the peak of the algorithm is compared with other six algorithms. The Dice similarity coefficient (volume overlap error) is higher (lower), indicating that the proposed algorithm has stronger robustness and segmentation ability.

In order to objectively evaluate the time efficiency of each algorithm execution, the above four algorithms are used to segment and test the four images in Fig. 6, and the time overhead of each algorithm is counted. The result is shown in Fig. 6. It can be seen from Fig. 6 that the time overhead of the proposed algorithm is similar to that of the PKFCM algorithm, but compared with the other five algorithms, the time cost of the algorithm is significantly reduced, and the operation efficiency is improved, which indicates that the algorithm has better real-time performance.

Conclusion

Medical image analysis plays an important role in computer-aided liver-carcinoma diagnosis. Aiming at the existing image fuzzy clustering segmentation being not suitable to segment CT image with non-uniform background, a fast robust kernel space fuzzy clustering segmentation algorithm is proposed. Firstly, the samples in European Space are mapped to the high

Table 2 Dice similarity coefficient (DSC) and volume overlap error (VOE) of different algorithms to suppress Gaussian noise

Models	FC-PFS	PFCM	FCPFS	PKFC	PFC	PKFCM	Proposed
Dice/%	0.7252	0.7217	0.6928	0.7198	0.6855	0.7138	0.7685
VOE/%	0.2851	0.2852	0.2616	0.3705	0.3325	0.3142	0.2512

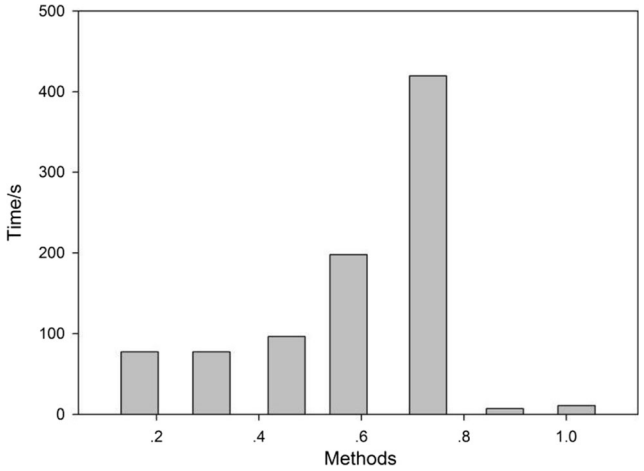

Fig. 6 Comparison of time cost of different algorithms

dimensional feature space through the kernel function. Then the linear weighted filtering image is obtained by combining the current pixel with its neighborhood pixels through the space information in the segmenting image. Finally, the two-dimensional histogram between the clustered pixels and its neighborhood mean is introduced into the robust kernel space image fuzzy clustering, and the iterative expression of the fast robust fuzzy clustering in kernel space is obtained by using Lagrange multiplier method. The experimental results on four databases show that our proposed method can segment liver tumors from abdominal CT volumes effectively and automatically, and the comprehensive segmentation performance of the proposed method is superior to that of several existing methods.

Compliance with ethical standards

Conflict of interest Author declares that he has no conflict of interest. Research involving human participants.

Informed consent Informed consent was obtained from all individual participants included in the study.

References

1. Campadelli, P., Casiraghi, E., and Esposito, A., Liver segmentation from computed tomography scans: A survey and a new algorithm. *Artif. Intell. Med.* 45(2–3):185–196, 2009.
2. Tomoshige, S., Oost, E., Shimizu, A. et al., A conditional statistical shape model with integrated error estimation of the conditions; application to liver segmentation in non-contrast CT images. *Med. Image Anal.* 18(1):130–143, 2014.
3. Peng, J., Wang, Y., and Kong, D., Liver segmentation with constrained convex variational model. *Pattern Recogn. Lett.* 43(7):81–88, 2014.
4. Qian, P., Jiang, Y., Deng, Z., Lingzhi, H., Sun, S., Wang, S., and Muzic, Jr., R. F., Cluster prototypes and fuzzy memberships jointly leveraged cross-domain maximum entropy clustering. *IEEE Transactions on Cybernetics* 46(1):181–193, 2016.
5. Yang, H., and Zeng, J. H., A hierarchical local region-based sparse shape composition for liver segmentation in CT scans. *Pattern Recogn.* 50:88–106, 2016.
6. Moghbel, M., Mashohor, S., Mahmud, R. et al., Review of liver segmentation and computer assisted detection/diagnosis methods in computed tomography. *Artif. Intell. Rev.*, 2017.
7. Norajitra, T., and Maier-Hein, K., 3D statistical shape models incorporating landmark-wise random regression forests for Omni-directional landmark detection. *IEEE Trans. Med. Imaging* 2016: 1–1.
8. Anca, C., Xavier, B., Olivier, C. et al., Semi-supervised segmentation of ultrasound images based on patch representation and continuous min cut. *PLoS One* 9(7):e100972, 2014.
9. Thong, P., Abolmaesumi, P., and Hashtrudi-Zaad, K., Intra-subject elastic registration of 3D ultrasound images. *Med. Image Anal.* 10(5):713–725, 2006.
10. Kang, X., Ren, H., Li, J. et al., Computer-assisted bone tumour ablation using sparse radiographs. *Adv. Robot.* 28(5):303–315, 2014.
11. Wuttisarnwattana, P., Gargesha, M., Hof, W. V. et al., Automatic stem cell detection in microscopic whole mouse Cryo-imaging. *IEEE Trans. Med. Imaging* 35(3):819–829, 2016.
12. Liu, J., Wang, S., Linguraru, M. G. et al., Tumor sensitive matching flow: A variational method to detecting and segmenting perihepatic and perisplenic ovarian cancer metastases on contrast-enhanced abdominal CT. *Med. Image Anal.* 18(5):725–739, 2014.
13. Hoogi, A., Subramaniam, A., Veerapaneni, R. et al., Adaptive estimation of active contour parameters using convolutional neural networks and texture analysis. *IEEE Trans. Med. Imaging* 36(3): 781–791, 2017.
14. Zheng, Y., Ai, D., Zhang, P. et al., Feature learning based random walk for liver segmentation. *PLoS One* 11(11):e0164098, 2016.
15. Qian, P., Zhao, K., Jiang, Y., Su, K.-H., Deng, Z., Wang, S., and Muzic, Jr., R. F., Knowledge-leveraged transfer fuzzy c-means for texture image segmentation with self-adaptive cluster prototype matching. *Knowl.-Based Syst.* 130:33–50, 2017.
16. Jiang, Y., Deng, Z., Chung, F.-L., Wang, G., Qian, P., Choi, K.-S., and Wang, S., Recognition of epileptic EEG signals using a novel multi-view TSK fuzzy system. *IEEE Trans. Fuzzy Syst.* 25(1):3–20, 2017.
17. Xuesong, L., Qinlan, X., Yunfei, Z. et al., Fully automatic liver segmentation combining multi-dimensional graph cut with shape information in 3D CT images. *Sci. Rep.* 8(1):10700–10712, 2018.
18. Mharib, A. M., Ramli, A. R., Mashohor, S. et al., Survey on liver CT image segmentation methods. *Artif. Intell. Rev.* 37(2):83–95, 2012.
19. Xiaomeng, L., Hao, C., Xiaojuan, Q. et al., H-DenseUNet: Hybrid densely connected UNet for liver and tumor segmentation from CT volumes. *IEEE Trans. Med. Imaging*:1–1, 2018.
20. Häme, Y., and Pollari, M., Semi-automatic liver tumor segmentation with hidden Markov measure field model and non-parametric distribution estimation. *Med. Image Anal.* 16(1):140–149, 2012.
21. Xia, K. J., Yin, H. S., and Wang, J. Q., A novel improved deep convolutional neural network model for medical image fusion. *Clust. Comput.* 28(3):1–13, 2018.
22. Chaieb, F., Ben Said, T., Mabrouk, S. et al., Accelerated liver tumor segmentation in four-phase computed tomography images. *J. Real-Time Image Proc.* 13(1):121–133, 2017.
23. Vorontsov, E., Tang, A., Roy, D. et al., Metastatic liver tumour segmentation with a neural network-guided 3D deformable model. *Med. Biol. Eng. Comput.* 55(1):127–139, 2017.
24. Smeets, D., Loeckx, D., Stijnen, B. et al., Semi-automatic level set segmentation of liver tumors combining a spiral-scanning technique with supervised fuzzy pixel classification. *Med. Image Anal.* 14(1):13–20, 2010.

25. Sun, C., Guo, S., Zhang, H. et al., Automatic segmentation of liver tumors from multiphase contrast-enhanced CT images based on FCNs. *Artif. Intell. Med.*:S0933365716305930, 2017.
26. Zygomalas, A., Karavias, D., Koutsouris, D. et al., Computer-assisted liver tumor surgery using a novel semiautomatic and a hybrid semiautomatic segmentation algorithm. *Med. Biol. Eng. Comput.* 54(5):711–721, 2016.
27. Xia, K.-j., Yin, H.-s., and Zhang, Y.-d., Deep semantic segmentation of kidney and space-occupying lesion area based on SCNN and ResNet models combined with SIFT-flow algorithm. *J. Med. Syst.* 43:2, 2019. https://doi.org/10.1007/s10916-018-1116-1.
28. Ruskó, L., Bekes, G., and Fidrich, M., Automatic segmentation of the liver from multi- and single-phase contrast-enhanced CT images. *Med. Image Anal.* 13(6):871–882, 2009.
29. Lee, W. L., Chen, Y. C., Chen, Y. C. et al., Unsupervised segmentation of ultrasonic liver images by multiresolution fractal feature vector. *Inf. Sci.* 175(3):177–199, 2005.
30. Hoogi, A., Beaulieu, C. F., Cunha, G. M. et al., Adaptive local window for level set segmentation of CT and MRI liver lesions. *Med. Image Anal.* 37(4):46–55, 2017.
31. Kaijian Xia, Hongsheng Yin, Pengjiang Qian, Yizhang Jiang, Shuihua Wang, Liver Semantic Segmentation Algorithm Based on Improved Deep Adversarial Networks in Combination of Weighted Loss Function on Abdominal CT Images. IEEE Access 7: 96349-96358 ,2019
32. Qian Zhao, Y., Hong Wang, X., Fang Wang, X. et al., Retinal vessels segmentation based on level set and region growing. *Pattern Recogn.* 47(7):2437–2446, 2014.
33. Tang, Z., Wang, S., Huo, J., Guo, H., Zhao, H., and Mei, Y., Bayesian framework with non-local and low-rank constraint for image reconstruction. *J. Phys. Conf. Ser.* 787(787):1–11, 2017.
34. Wang, G., Zhang, S., Xie, H. et al., A homotopy-based sparse representation for fast and accurate shape prior modeling in liver surgical planning. *Med. Image Anal.* 19(1):176–186, 2015.
35. Qian, P., Jiang, Y., Wang, S., Su, K.-H., Wang, J., Hu, L., and Muzic, Jr., R. F., Affinity and penalty jointly constrained spectral clustering with all-compatibility, flexibility, and robustness. *IEEE Transactions on Neural Networks and Learning Systems* 28(5): 1123–1138, 2017.
36. Jiang, Y., Chung, F.-L., Wang, S., Deng, Z., Wang, J., and Qian, P., Collaborative fuzzy clustering from multiple weighted views. *IEEE Transactions on Cybernetics* 45(4):688–701, 2015.
37. Jiang, Y., Chung, F.-L., Ishibuchi, H. et al., Multitask TSK fuzzy system modeling by mining intertask common hidden structure. *IEEE Transactions on Cybernetics* 45(3):548–561, 2015.
38. Kajian, X., Jiangqiang, W., and Yue, W., Robust Alzheimer disease classification based on feature integration fusion model for magnetic[J]. *Journal of Journal of medical imaging and health informatics* 24(7):1–6, 2017.

Publisher's Note Springer Nature remains neutral with regard to jurisdictional claims in published maps and institutional affiliations.